J Mol Model (2013) 19:1435–1444
DOI 10.1007/s00894-012-1698-3

ORIGINAL PAPER

Fluorescent sensors based on BODIPY derivatives for aluminium ion recognition: an experimental and theoretical study

Tasawan Keawwangchai · Nongnit Morakot · Banchob Wanno

Received: 25 July 2012 / Accepted: 14 November 2012 / Published online: 9 December 2012

Abstract Two BODIPY derivative sensors for metal ion recognition containing 10-(4-hydroxyphenyl) (**L1**) and 10-(3,4-dihydroxyphenyl) (**L2**) were synthesized in a one-pot reaction of benzaldehyde derivative and 2,4-dimethylpyrrole in the presence of trifluoroacetic acid as catalyst. The binding abilities between these sensors and 50 equivalents of Na^{+}, K^{+}, Ag^{+}, Ca^{2+}, Fe^{2+}, Co^{2+}, Ni^{2+}, Cu^{2+}, Zn^{2+}, Cd^{2+}, Pb^{2+}, Al^{3+} and Cr^{3+} ions were studied using UV–vis and fluorescent spectroscopic methods. Of all the metal ions tested, Al^{3+} ion showed the greatest decrease in intensity in the spectra of the sensors, and therefore Al^{3+} ion forms the strongest complex. The binding abilities of BODIPY receptors with Na^{+}, Ag^{+}, Ca^{2+}, Co^{2+}, Ni^{2+}, Cu^{2+}, Zn^{2+} and Al^{3+} ions were also investigated using density functional theory (DFT) calculations at B3LYP/LanL2DZ theoretical level. The calculated results point to the same conclusion. DFT calculations also provided the HOMO–LUMO energy levels, which can explain the spectrum change upon complexation.

Keywords Aluminium · BODIPY · DFT · Fluorescence · PET · Receptor · Sensor

Introduction

The design of selectively fluorescent sensors capable of recognizing metal ions has attracted much interest in recent years, especially fluorescent sensors for analytical purposes [1–4]. Their design consists of two parts: a receptor subunit, a unit responsible for selectivity; and a fluorescent molecule subunit, a unit responsible for signaling. In most cases, the receptor subunit and fluorescent molecule are covalently attached to form a fluorescence sensor. The fluorescent molecule can be chosen from various organic fluorescent dyes such as rhodamine [5], fluorescein [6], naphthalimide [7], and 4,4-difluoro-4-bora-3a,4a-diaza-*s*-indacene (BODIPY)s [8].

Among them, BODIPY is a very attractive signaling subunit for the construction of sensors because of its robustness against light and chemicals, relatively high molar absorption coefficients and high fluorescent quantum yield, narrow emission bandwidth, good solubility, resistance towards self aggregation in solution, relatively longer excitation/emission wavelength characteristics and short fluorescent lifetime. Moreover, their spectroscopic and photophysical properties can be fine-tuned by attachment of ancillary residues at the appropriate positions of the difluoroboron dipyrromethene core [9–12]. These excellent properties have resulted in the widespread use of BODIPY-based sensor in many fields of biological systems, such as monitoring cholesterol in living cells [13], the presence of an amino acid moiety in proteins [14], and hepatitis C virus (HCV) activity [15]. Other applications include laser dyes [16], nanocrystals [17], and fluorescent switches [18] and receptors [19]. Recently, many BODIPY-based receptors have been reported as metal ion recognition. The mechanism responsible for BODIPY-based sensing is photoinduced electron transfer (PET) [20, 21]. In principle, PET can take place in two directions: from a donor to the excite-state fluorophore (reductive PET), or from an excite-state fluorophore to a receptor (oxidative PET). Both events are accompanied by a quenching of the fluorophore emission.

Electronic supplementary material The online version of this article (doi:10.1007/s00894-012-1698-3) contains supplementary material, which is available to authorized users.

T. Keawwangchai · N. Morakot (✉) · B. Wanno (✉)
The Center of Excellence for Innovation in Chemistry (PERCH–CIC) and Supramolecular Chemistry Research Unit, Department of Chemistry, Faculty of Science, Mahasarakham University, Maha Sarakham 44150, Thailand
e-mail: m.nongnit@gmail.com
e-mail: banchobw@gmail.com

The present work focused on the design and synthesis of BODIPY-based fluorescence sensors for metal ions. Target fluorescence sensors were designed to contain BODIPY moiety as fluorescence signaling subunit. The 4-hydroxyphenyl (**L1**) and 3,4-dihydroxyphenyl (**L2**) groups at BODIPY meso-position were proposed for the metal ion binding subunit. The binding properties of the complexation between sensors and metal ions (Na^+, K^+, Ag^+, Ca^{2+}, Fe^{2+}, Co^{2+}, Ni^{2+}, Cu^{2+}, Zn^{2+}, Cd^{2+}, Pb^{2+}, Al^{3+} and Cr^{3+}) were investigated by UV–vis and fluorescent spectrophotometry. Computational calculations were performed to give an insight in explaining the behavior of synthetic fluorescent sensors and the complexation of metal ions. The computation included geometrical structures and binding energies, and the thermodynamic property changes of complexation between sensors with Na^+, Ag^+, Ca^{2+}, Co^{2+}, Ni^{2+}, Cu^{2+}, Zn^{2+} and Al^{3+} ions were calculated using the density functional theory (DFT) method.

Methods

General considerations

Unless otherwise specified, all materials were reagent grade, purchased from Fluka (Buchs, Switzerland), BDH (https://us.vwr.com/store), Aldrich (St. Louis, MO), Carlo Erba (http://www.carloerbareagents.com/), Merck (Darmstadt, Germany) or J.T. Baker (http://www.jtbaker.nl/index.htm) and used without further purification. Commercial grade solvents, such as acetone, dichloromethane, hexane, methanol and ethylacetate were purified by distillation before use. Acetonitrile and dichloromethane for reaction work were dried over calcium hydride and freshly distilled under nitrogen atmosphere. All reactions were carried out under nitrogen atmosphere before use. Analytical thin-layer chromatography was carried out with silica gel plates (Kieselgel 60, F_{254}, 1 mm, Merck; supported on aluminum); detection was by UV lamp (254 and 365 nm). Column chromatography was carried out on silica gel (Kieselgel 60, 0.063–0.200 nm, Merck). Nuclear magnetic resonance (NMR) spectra were recorded on Varian 400 MHz nuclear magnetic resonance spectrometer. In all cases, sensors were dissolved in deuterated chloroform ($CDCl_3$). Matrix-assisted laser desorption ionization time of flight mass spectra (MALDI-TOF MS) were determined on a Bruker Daltonics instrument (http://www.bruker.com/), using acetonitrile as solvent. UV–vis spectra were measured by a Perkin Elmer Lambda 25 spectrophotometer at 25 °C (http://www.perkinelmer.co.uk). Fluorescent spectra were recorded on a Perkin Elmer SL50B fluorescence spectrophotometer with excitation and emission slit set at 5.0 nm.

Synthesis

5,5-difluoro-10-(4-hydroxyphenyl)-1,3,7,9-tetramethyl-5H-dipyrrolo[1,2-c:2',1'-f][1–3]diazaborinin-4-ium-5-uide, **L1**

4-Hydroxybenzaldehyde, **1** (310 mg, 0.75 mmol) and 2,4-dimethylpyrrole (3 ml, 2 mmol) were dissolved in anhydrous methylene chloride (160 ml) under nitrogen atmosphere. One drop of trifluoroacetic acid (TFA) was then added to the solution, which was then stirred for 5 h at room temperature (RT). A solution of 2,3-dichloro-5,6-dicyano-1,4-benzoquinone (DDQ, 360 mg, 2.16 mmol) in CH_2Cl_2 was added using an addition funnel, and the reaction was continued for another 4 h. Then, 2 ml triethylamine (Et_3N) was added, followed by 4 ml BF_3OEt_2 during 30 min, and stirred overnight. The mixture was concentrated in vacuo, water (50 ml) was added, and the organic layer was separated, washed with water, and dried (anhydrous Na_2SO_4). After concentrated in vacuo, the residue was purified by column chromatography (silica, CH_2C1_2/MeOH, 9.9/0.1, v/v). The desired product **L1** was obtained as greenish-red solid (130 mg, 37 % yield). ^{1}H-NMR spectrum (400 MHz, $CDCl_3$): δ 1.44 (s, 6H, C*H*$_3$-pyrrole), 2.55 (s, 6H, C*H*$_3$-pyrrole), 5.19 (s, 1H, *H*O-phenol), 5.98 (s, 2H, *H*-pyrrole), 6.94 (d, 2H J=8.4 Hz, C_6H_5), 7.12 (d, 2H J=8.4 Hz, C_6H_5). ^{13}C-NMR spectrum (400 MHz, $CDCl_3$, ppm): δ 14.1, 14.7, 116.9, 121.4, 124.1, 129.3, 131.3, 142.7, 154.7, 158.5. MALDI-TOF MS (m/z) calcd. $[M]^+$ for $C_{19}H_{18}BF_2N_2O$ 339.148, found 339.549.

10-(3,4-dihydroxyphenyl)-5,5-difluoro-1,3,7,9-tetramethyl-5H-dipyrrolo[1,2-c:2',1'-f][1–3]diazaborinin-4-ium-5-uide, **L2**

The **L2** sensor was synthesized using the same procedure as for **L1** synthesis but using 3,4-dihydroxybenzaldehyde, **2** as the starting material. After completing the reaction, the residue was purified by column chromatography (silica, CH_2C1_2/MeOH, 9.5/0.5, v/v). The desired product **L2** was obtained as a red solid (136 mg, 36 % yield). ^{1}H-NMR spectrum (400 MHz, $CDCl_3$): δ 1.49 (s, 6H, C*H*$_3$-pyrrole), 2.53 (s, 6H, C*H*$_3$-pyrrole), 5.96 (s, 2H, *H*-pyrrole), 6.65 (d, J=8.4 Hz, 1H, C_6H_5), 6.74 (s, 1H, C_6H_5), 6.96 (d, J=8.0 Hz, 1H, C_6H_5). ^{13}C-NMR spectrum (400 MHz, $CDCl_3$, ppm): δ 13.7, 14.1, 21.6, 28.2, 114.5, 116.2, 116.3, 118.3, 120.7, 124.5, 131.3, 142.3, 146.5, 146.7, 154.0. MALDI-TOF MS (m/z) calcd. $[M]^+$ for $C_{19}H_{19}BF_2N_2O_2$ 355.143, found 355.682.

Computational details

Structures of BODIPY-based sensors and their complexes with metal ion guests i.e., Na^+, Ag^+, Ca^{2+}, Co^{2+}, Ni^{2+},

Cu^{2+}, Zn^{2+} and Al^{3+} were optimized in vacuo by using the DFT method. Calculations with hybrid density functional B3LYP recommended the Becke's three-parameter exchange functional [22] with the Lee-Yang-Parr correlation functional, [23] using the Los Alamos LanL2DZ split-valence basis set [24–26]. All calculations were performed using the GAUSSIAN 03 program [27]. The electronic properties of the BODIPY derivatives and their metal ion complexes were analyzed. The highest occupied molecular orbital (HOMO), singly occupied molecular orbital (SOMO), the lowest unoccupied molecular orbital (LUMO) and the energy gaps referred to the energy difference between HOMO and LUMO orbitals ($\Delta E_{HOMO-LUMO}$) or SOMO and LUMO orbitals ($\Delta E_{SOMO-LUMO}$) were also investigated at the same level of theory. Thermodynamic property changes (ΔX) i.e., total energy (ΔE), enthalpy (ΔH) and Gibbs free energy (ΔG) changes, of complexation in the fully optimized geometries were obtained from the following equation:

$$\Delta X = X(\text{sensor/M}) - [X(\text{sensor}) + X(\text{M})]$$

where X(sensor/M), X(sensor) and X(M) are the thermodynamic properties of the sensor/metal ion complex, free sensor and metal ion, respectively. In addition, natural bond orbital (NBO) analysis implemented in the GAUSSIAN 03 program was applied through a series of intermolecular interactions under the above system to evaluate NBO charges.

Results and discussion

Synthesis

The present work aimed at designing and synthesizing the metal ion sensors containing BODIPY dye giving an optical signal. Hydroxyl phenyl moieties were used as metal ion binding sites in receptor subunits. The BODIPY fluorophore was linked directly to the receptor subunits. The synthetic pathway is shown in Scheme 1.

The related BODIPY derivatives **L1** and **L2** were previously synthesized for pH and redox active metal studies, but the synthesis involved a multistep pathway [28, 29]. In the present work, **L1** and **L2** sensors were synthesized by a simpler one-pot reaction modified according to the procedure reported by Gabe and co-workers [30]. The condensation reaction of benzaldehyde derivative and 2,4-dimethylpyrrole in the present of TFA as catalyst was carried out in anhydrous methylene chloride under nitrogen atmosphere. After oxidization by DDQ followed by reaction with BF_3OEt_2, the residue was purified by column chromatography. The desired product **L1** was obtained as greenish-red solid in 37 % yield, and **L2** was obtained as a red solid in 36 % yield.

Spectroscopic and detective properties

The absorption and fluorescent spectra of **L1** and **L2** sensors (Fig. 1) show the characteristic spectroscopic properties of the BODIPY chromophore with slight stroke shifts. In methanol, a strong S_0–S_1 transition with maximum at 497 nm (ε=90,800 $M^{-1}cm^{-1}$ and ε=39,400 $M^{-1}cm^{-1}$ for **L1** and **L2**, respectively) and a shoulder at shorter wavelengths are observed [31]. The fluorescent spectra of both **L1** and **L2** sensors display an emission at 509 and 515 nm, respectively. The fluorescent intensity is very high for **L1** but low for the analogous **L2** upon excitation at 485 nm due to the PET process from the hydroxyphenyl moiety to the BODIPY fluorophore [32]. The quantum yield of **L2** is lower than that of **L1** because **L2** has two electron donor atoms that form two hydroxyl groups that allow the PET process to proceed more easily.

Preliminary studies on the selectivity of BODIPY-based sensors **L1** (1.0×10^{-5}M) and **L2** (1.0×10^{-5}M) with the addition of 50 equivalents of various metal ions such as Na^+, K^+, Ag^+, Ca^{2+}, Fe^{2+}, Co^{2+}, Ni^{2+}, Cu^{2+}, Zn^{2+}, Cd^{2+}, Pb^{2+}, Al^{3+} and Cr^{3+} in dry methanol were investigated by UV–vis spectrophotometry. The spectra were recorded from 400 to 900 nm at ambient temperature. The spectroscopic properties of free sensors **L1**, **L2** and their metal ion complexations are shown in Fig. 2. The absorption spectra of sensors **L1** and **L2** in the free and complexed forms of metal ions are displayed in Fig. 2a, b. Both

Scheme 1 Synthesis of BODIPY-based sensors **L1** and **L2**

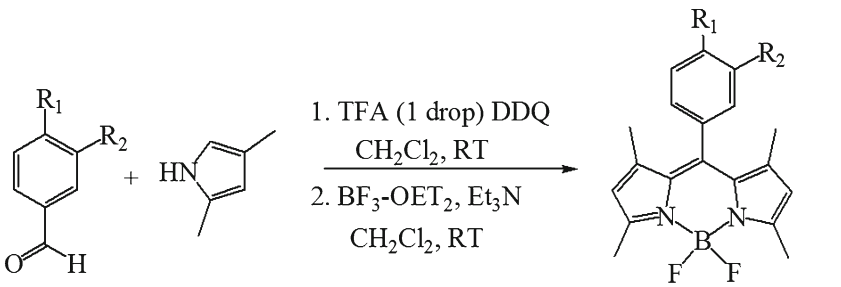

1 R_1= OH, R_2= H
2 R_1= OH, R_2= OH

L1 R_1= OH, R_2= H
L2 R_1= OH, R_2= OH

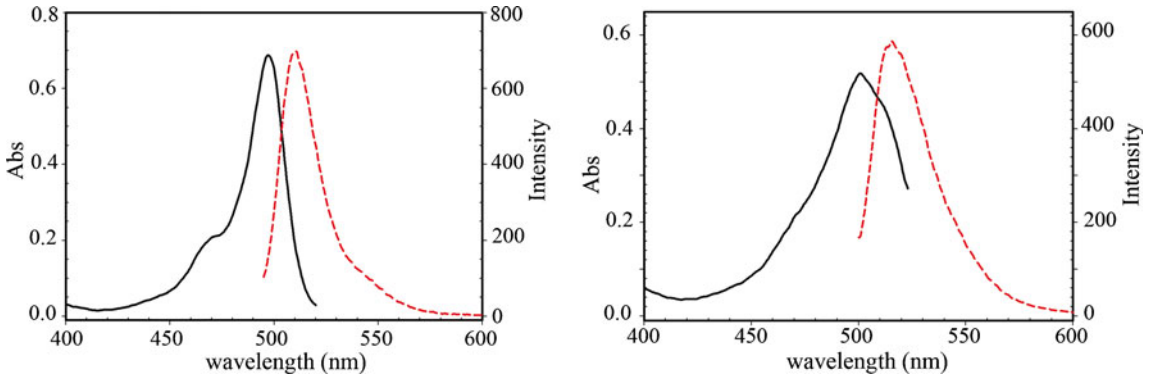

Fig. 1 Absorption (*solid line*) and fluorescent (*dotted line*) spectra of sensors **L1** (*left*) and **L2** (*right*) in dry methanol

sensors **L1** and **L2** show an absorption band centered at 497 nm. After addition of metal ions to the sensor solution, the intensity of the absorption spectra decreased, particularly for the Al^{3+} ion (ε=63,600 $M^{-1}cm^{-1}$).

The fluorescent behavior between synthetic sensors and excess metal ions of the complexes in dry methanol was also investigated (λ_{ex} at 485 nm, λ_{em} 490–600 nm). The fluorescence spectra of **L1** (1.0×10^{-7}M) and **L2** (1.0×10^{-5}M) in the presence and absence of various metal ions are displayed in Fig. 2c, d. Upon addition of 50 equivalents of Al^{3+} ion, the intensity of the emission band at 509 nm decreased dramatically. The quenching extent of sensors **L1** and **L2** toward Al^{3+} ion was estimated to be 6-fold (Φ_0/Φ=5.948) and 2-fold (Φ_0/Φ=1.882), respectively. Interestingly, the fluorescence intensity of **L1** was not decreased significantly by the addition of other metal ions. Therefore, sensors **L1** and **L2** have potential to be used as selective fluorescence sensors for Al^{3+} ion. The decreasing fluorescence intensity

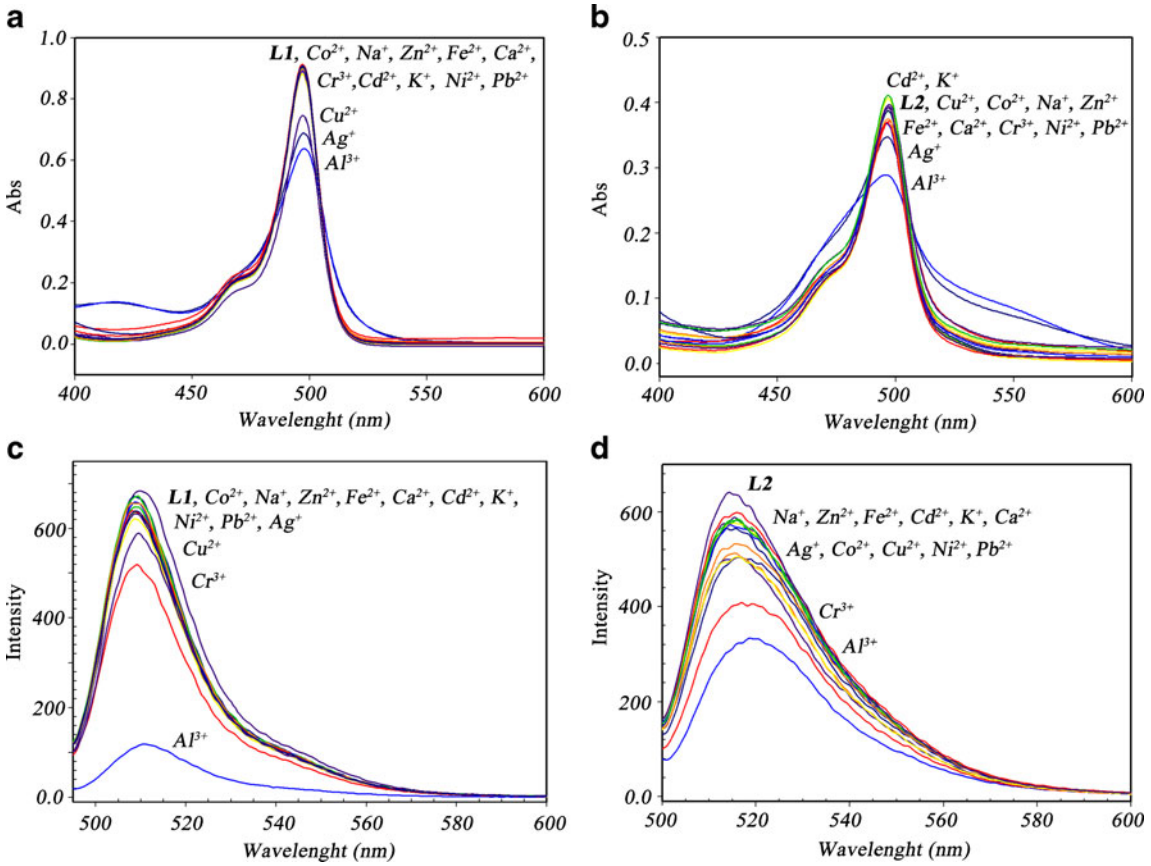

Fig. 2a–d The spectroscopic properties of free sensors **L1**, **L2** and their metal ion complexations (50 equivalents) in dry methanol. **a** UV–vis spectrum changes of sensor **L1** (1.0×10^{-5}M). **b** UV–vis spectrum changes of sensor **L2** (1.0×10^{-5}M). **c** Fluorescence spectrum changes of sensor **L1** (1.0×10^{-7}M). **d** Fluorescence spectrum changes of sensor **L2** (1.0×10^{-5}M)

of sensors **L1** and **L2** upon addition of Al^{3+} ion could be described by the hard soft acid base (HSAB) principle [33]. The Al^{3+} ion, with its relatively small radius and high ionic charge, is a hard metal ion, and thus prefers to form stable complexes with the oxygen atoms (the hard donor atoms or hard donor bases) of hydroxyl groups of receptors. The strong HSAB Cr^{3+} ion has a small radius and high charge but its fluorescence quenching is less than that of the Al^{3+} ion. This phenomenal can be explained by the ionic size of Al^{3+}, which is smaller than Cr^{3+} (53 pm Al^{3+} vs 76 pm Cr^{3+}) while the absolute hardness parameter of Al^{3+} is higher than that of Cr^{3+} (119.99 eV Al^{3+} vs 49.1 eV Cr^{3+}) [34].

Geometrical structures

The chemical and graphical structures and atomic labeling of **L1** and **L2** complexes with metal ions are displayed in Fig. 3. The intensive DFT method at the B3LYP/LanL2DZ theoretical level was chosen for optimization of the structures of **L1** and **L2** and their complexes with metal ions [35–38]. All calculations were obtained in vacuo, and the optimized structures are shown in Figs. 4 and 5. The selected geometrical parameters of the data of all optimized structures are listed in Tables S1 and S2. The complexations of **L1** and **L2** with metal ions revealed the remarkable change in **L1** and **L2** structures. In detail, the C4–O1 bond lengths of **L1**/metal ion complexes are longer than the C4-O1 bond length (1.399 Å) of free **L1,** whereas C3-O2 and C4-O1 bond lengths of **L2**/metal ion complexes are also longer than the C3-O2 and C4-O1 bond lengths (1.394 Å) of free **L2**. Moreover, the N1-B and N2-B bond lengths of metal ion complexes of both **L1** and **L2** are shorter than N1-B and N2-B bond lengths (1.534 Å) of free **L1** and **L2**. The N1-B-N2 bond angles of metal ion complexes with **L1** and **L2** are smaller compared with the N1-B-N2 bond angles (108.3 Å) of free **L1** and **L2**. Clearly, metal ion recognition via ion-dipole interactions causes a change in structural properties not only of hydroxyl phenyl receptor moieties but also of the BODIPY fluorophore.

Thermodynamic property changes

The most important parameter in the evaluation of selectivity of a sensor toward a metal ion is the binding strength, which is reflected in the binding energy, binding enthalpy, and Gibbs free energy. The calculated values of these parameters are listed in Table 1. The binding strengths for **L1** and metal ions decrease in the order: **L1**/Al^{3+} > > **L1**/Cu^{2+} > **L1**/Ni^{2+} > **L1**/Zn^{2+} > **L1**/Co^{2+} > > **L1**/Ca^{2+} > **L1**/Ag^{+} > **L1**/Na^{+}. For **L2**, the binding strengths of **L2** and metal ions decrease in the order: **L2**/Al^{3+} > > **L2**/Cu^{2+} > **L2**/Co^{2+} > **L2**/Ni^{2+} > **L2**/Na^{+} > **L2**/Zn^{2+} > > **L2**/Ca^{2+} > **L2**/Ag^{+}. The selectivity is also highest for the Al^{3+} ion. Therefore, both sensors **L1** and **L2** show the highest selectivity toward Al^{3+} ion, which agrees well with experimental results. For all metal ions, the calculation enthalpies show that complexation is an exothermic process.

Electronic properties and partial charge transfers

The electronic properties of **L1** and **L2** and their metal ion complexes were computed at the B3LYP/LanL2DZ level of theory. The NBO charges were also computed, and NBO charges of the selected atoms are listed in Table 2. The charges on hydroxyphenyl receptor moieties and BODIPY fluorophore subunit changed when bound with metal ions. These results indicate that the metal ion recognition, which occurring via an ion–dipole interaction, induced a charge transfer process not only from hydroxyphenyl receptor moieties to the metal ion but also from the BODIPY fluorophore. The metal to ligand charge transfers (MLCT) are presented as a bar graph in Fig. 6. The complexation of Al^{3+} ion shows the highest MLCT for both receptors **L1** and **L2**. The MLCT properties of **L1** and **L2** receptors showed similar trends for all metal ions except Ag^{+} and Co^{2+}. This

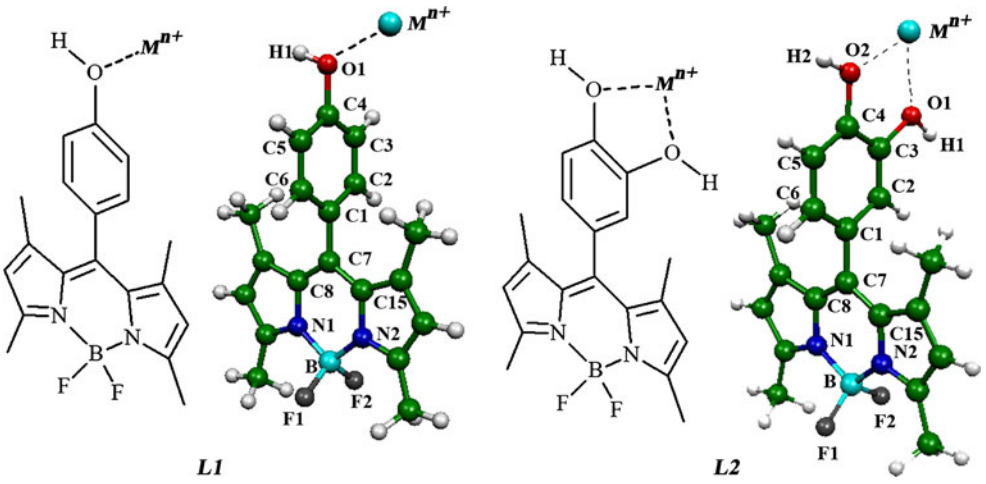

Fig. 3 The chemical and graphical structures and atomic labeling of sensors **L1** and **L2** complexes with metal ions

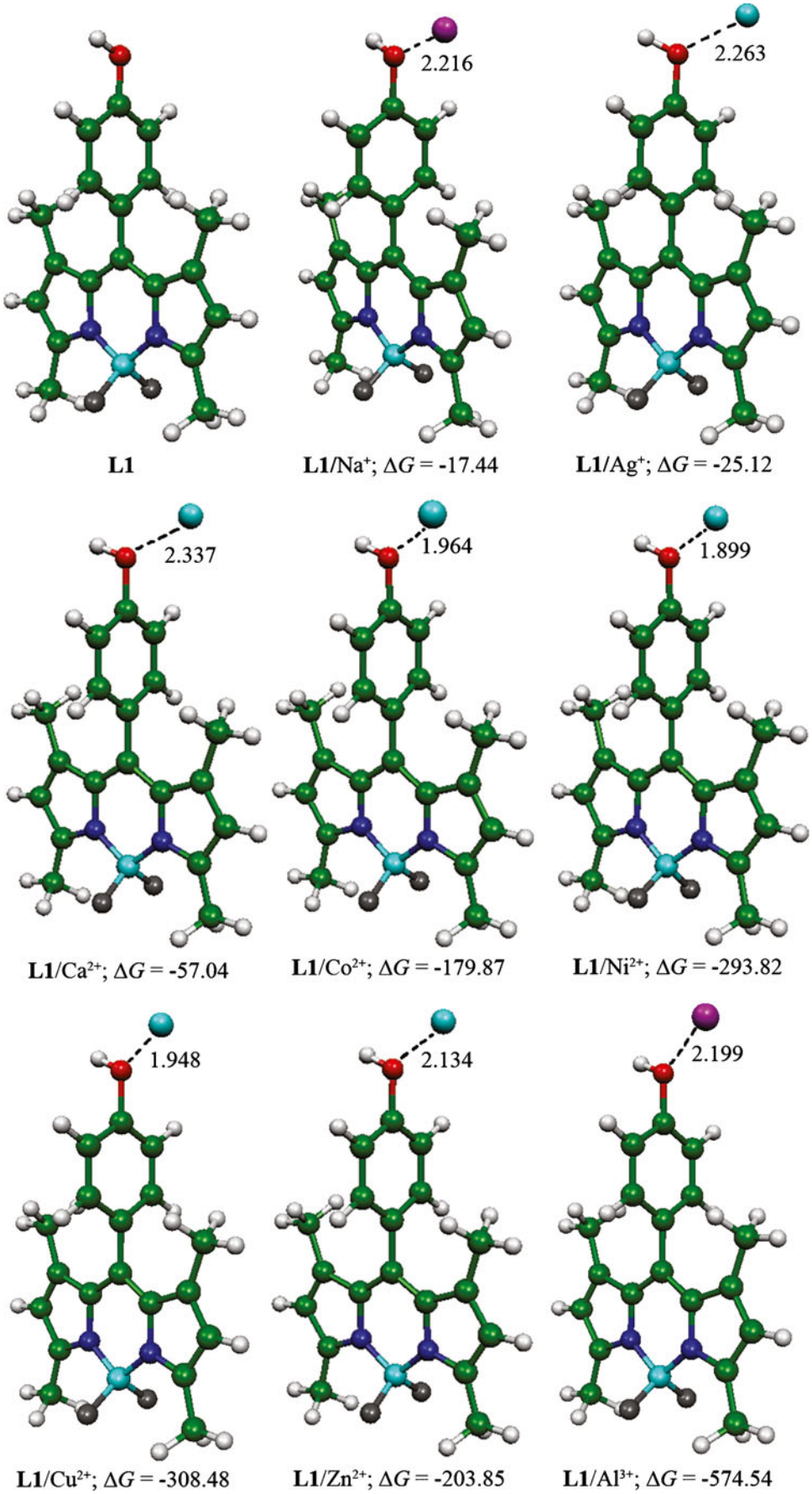

Fig. 4 The B3LYP/LanL2DZ optimized structures of sensor **L1** and its metal ion complexes. The presented bond distances and binding free energies are in Å and kcal mol^{-1}, respectively

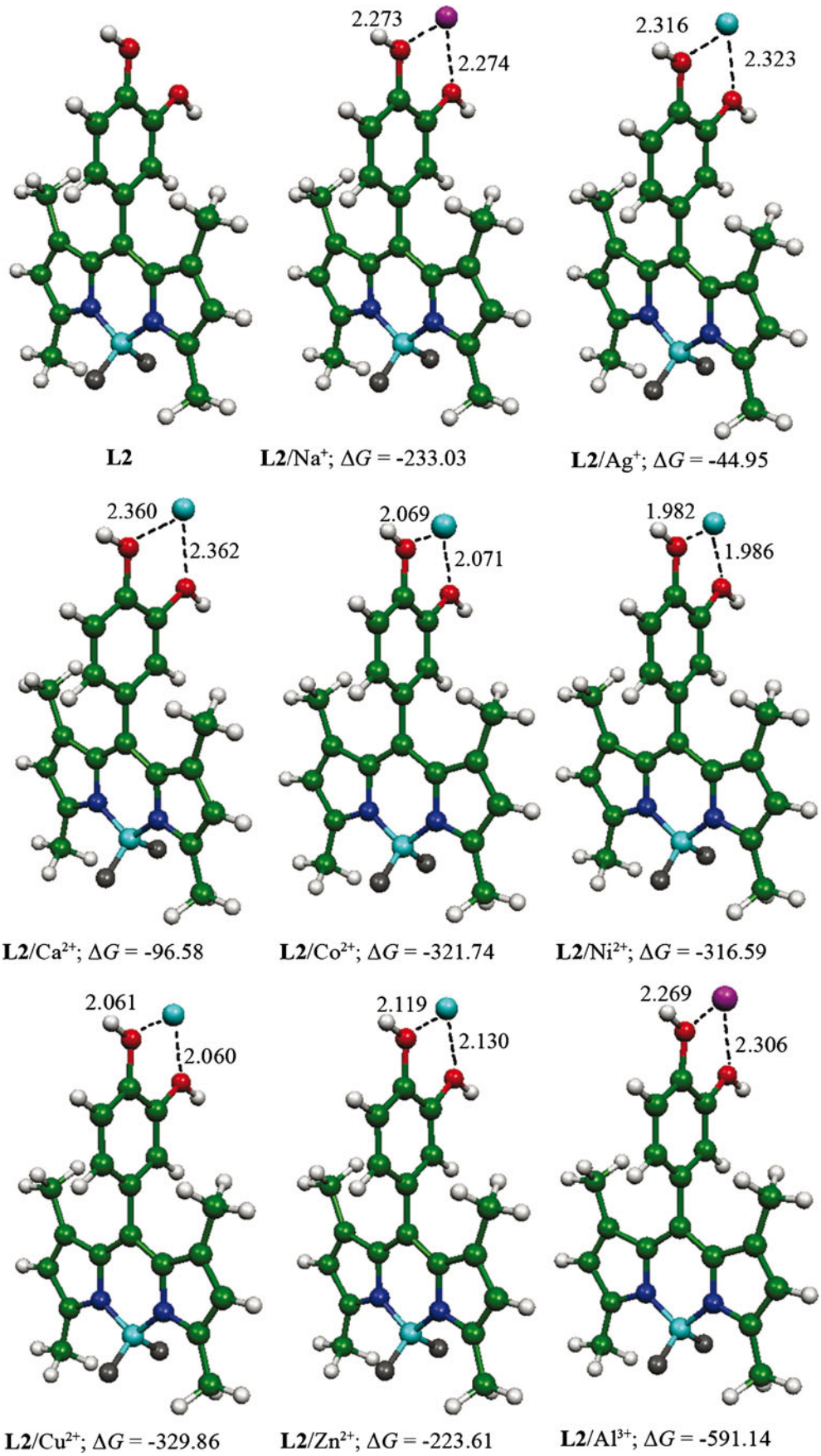

Fig. 5 The B3LYP/LanL2DZ optimized structures of sensor **L2** and its metal ion complexes. The presented bond distances and binding free energies are in Å and kcal mol^{-1}, respectively

Table 1 The zero point vibrational correction energy (ΔE_{ZPE}) and enthalpy (ΔH) and Gibbs free energy (ΔG) changes of complexes between sensors **L1**, **L2** and metal ions computed at B3LYP/LanL2DZ level of theory

Metal ion	ΔE_{ZPE} [a]		ΔH [a]		ΔG [a]	
	L1	**L2**	**L1**	**L2**	**L1**	**L2**
Na^+	−21.58	−252.08	−25.33	−269.86	−17.44	−233.03
Ag^+	−29.99	−49.87	−33.60	−52.90	−25.12	−44.95
Ca^{2+}	−61.94	−101.21	−66.23	−104.54	−57.04	−96.58
Co^{2+}	−188.38	−327.16	−193.91	−330.39	−179.87	−321.74
Ni^{2+}	−300.07	−321.93	−304.30	−325.14	−293.82	−316.59
Cu^{2+}	−313.48	−335.13	−317.20	−338.29	−308.48	−329.86
Zn^{2+}	−208.73	−228.69	−212.30	−231.82	−203.85	−223.61
Al^{3+}	−578.39	−595.36	−581.83	−598.27	−574.54	−591.14

[a] In kcal mol^{-1}

behavior may stem from the difference in electronic configuration. The Co^{2+} has a d^7 configuration while other transition metals have a d^8–d^{10} configuration. For Ag^+ ion, the geometry of the silver complex was limited to its linear structure while the geometries of other metal ions were not limited. The MLCT results agree well with the binding ability obtained from the theoretical and the experimental study.

The E_{LUMO}, E_{HOMO} or E_{SOMO} and $\Delta E_{HOMO–LUMO}$ or $\Delta E_{SOMO–LUMO}$ for **L1**, **L2** and their metal ion complexes are listed in Table S3. Experimental observation shows that, after being combined with metal ions, both **L1** and **L2** exhibit a dramatic decrease in the intensity of the emission band, which implies that the electron transfer process was greatly suppressed in the complexes. In order to appreciate the PET process from the fluorescent emission experiment, it was instructive to analyze the energy level of the corresponding molecular orbitals (MO) as first developed by Weller [39]. According to Weller's approach, after photo-inducing electronic excitation from occupied orbitals to unoccupied orbitals, the HOMO–LUMO electron distribution was computed on the total system. The donor and acceptor orbitals were distinguished simply by inspecting the orbital distribution diagram.

The orbital distribution diagrams of free receptor **L1** and **L1**/Al^{3+} and **L1**/Na^+ complexes are displayed in Fig. 7. The simple pathway of fluorescent emission and electron transfer processes of free receptor **L1** is displayed on the left of

Table 2 Selected natural bond orbital (NBO) charges (in *e*) of metals in **L1** and **L2** complexes computed at the B3LYP/LanL2DZ level of theory

Complex	N1[a]	N2[a]	B[a]	F1[a]	F2[a]	O1[a]	O2[a]	H1[a]	H2[a]	M[b]
L1	−0.629	−0.629	1.312	−0.580	−0.581	−0.729	–	0.493	–	–
L1/Na^+	−0.624	−0.622	1.310	−0.574	−0.574	−0.884	–	0.532	–	0.988
L1/Ag^+	−0.626	−0.625	1.309	−0.571	−0.571	−0.861	–	0.542	–	0.764
L1/Ca^{2+}	−0.628	−0.625	1.305	−0.559	−0.560	−0.941	–	0.556	–	1.403
L1/Co^{2+}	−0.631	−0.632	1.291	−0.545	−0.545	−0.821	–	0.526	–	0.141
L1/Ni^{2+}	−0.633	−0.633	1.301	−0.552	−0.552	−0.852	–	0.565	–	0.788
L1/Cu^{2+}	−0.633	−0.631	1.302	−0.553	−0.553	−0.908	–	0.565	–	0.935
L1/Zn^{2+}	−0.634	−0.634	1.301	−0.552	−0.552	−0.892	–	0.557	–	0.795
L1/Al^{3+}	−0.633	−0.634	1.293	−0.534	−0.534	−0.924	–	0.566	–	0.974
L2	−0.629	−0.629	1.311	−0.580	−0.581	−0.713	−0.712	0.493	0.492	–
L2/Na^+	−0.624	−0.624	1.310	−0.573	−0.575	−0.821	−0.821	0.527	0.526	0.975
L2/Ag^+	−0.624	−0.624	1.310	−0.573	−0.574	−0.834	−0.834	0.543	0.542	0.935
L2/Ca^{2+}	−0.625	−0.625	1.305	−0.560	−0.563	−0.892	−0.891	0.553	0.554	1.583
L2/Co^{2+}	−0.633	−0.633	1.301	−0.552	−0.553	−0.823	−0.822	0.555	0.558	0.917
L2/Ni^{2+}	−0.631	−0.632	1.301	−0.553	−0.554	−0.815	−0.814	0.564	0.567	0.914
L2/Cu^{2+}	−0.633	−0.633	1.301	−0.552	−0.553	−0.837	−0.836	0.556	0.559	0.937
L2/Zn^{2+}	−0.554	−0.632	1.301	−0.554	−0.554	−0.858	−0.859	0.562	0.565	1.039
L2/Al^{3+}	−0.634	−0.634	1.293	−0.535	−0.533	−0.833	−0.839	0.562	0.569	0.951

[a] N1, N2, B, F1, F2, O1, O2, H1 and H2 are atoms on sensors **L1** and **L2**, as defined in Fig. 3

[b] M is the metal ion on the complexes of **L1** and **L2**, as defined in Fig. 3

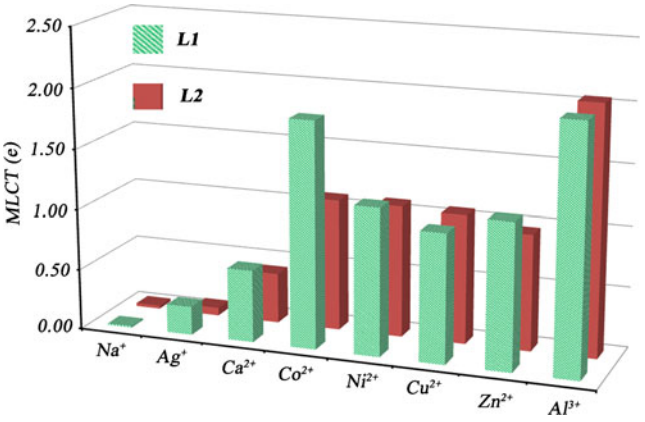

Fig. 6 Metal to ligand charge transfers (MLCT) of sensors **L1** and **L2** after attachment of metal ions

Fig. 7. To obtain these orbital energies, the electron distribution was picked out. The orbitals localized mainly on the BODIPY fluorophore part, as presented in the left column; similarly, the right column comes from orbitals distributed mainly on the hydroxyphenyl receptor part. The largest fluorescent emission quenching of **L1** by Al^{3+} ion addition can be explained by the reductive-PET mechanism (Fig. 7, middle). The HOMO of the BODIPY fluorophore is lower than that of the hydroxyphenyl receptor caused by the BODIPY fluorophore, which serves as the electron acceptor, so that an electron on the hydroxyphenyl receptor is capable of transferring to the BODIPY fluorophore and filling in the singly occupied HOMO. Accordingly, the above process is addressed as an oxidative-PET process. The complexation of sensor **L1** and Na^+ is based on an oxidative-PET process (Fig. 7, right). The LUMO of **L1**/Al^{3+} complex is very low comparing with the **L1**/Na^+ complex, indicating that the **L1**/Al^{3+} complex shows a stronger electron acceptor, easier electron transfer, and lower emission intensity in the fluorescent experiment than the **L1**/Na^+ complexes.

Conclusions

Two BODIPY derivatives containing 10-(4-hydroxyphenyl), **L1** and 10-(3,4-dihydroxyphenyl), **L2** were designed and synthesized for metal ion recognition. A one-pot reaction of benzaldehyde derivative and 2,4-dimethylpyrrole in the presence of TFA as catalyst was modified for the synthesis of these sensors. The binding abilities between synthetic sensors and 50

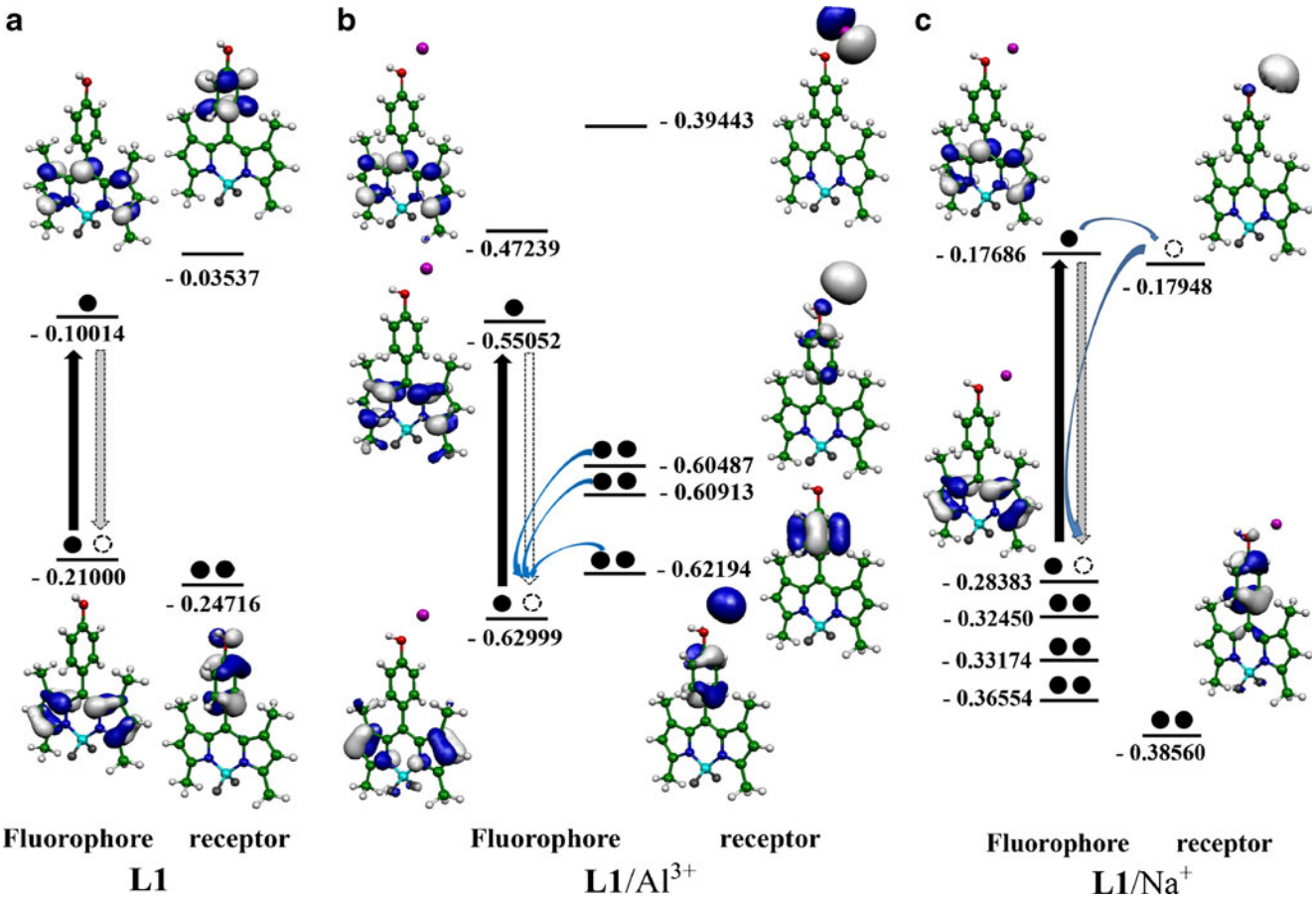

Fig. 7 Frontier orbital energy diagrams and electron-transfer paths in **a** **L1**, **b** **L1**/Al^{3+} and **c** **L1**/Na^+

equivalents of Na^+, K^+, Ag^+, Ca^{2+}, Fe^{2+}, Co^{2+}, Ni^{2+}, Cu^{2+}, Zn^{2+}, Cd^{2+}, Pb^{2+}, Al^{3+} and Cr^{3+} ions in methanol were studied using UV–vis and fluorescent spectrophotometric methods. The UV–vis and fluorescence spectra revealed a remarkable decrease in intensity when Al^{3+} ion was complexed with both sensors **L1** and **L2**, which can be explained by the HSAB principle. The optimized structures and thermodynamic properties of free **L1**, **L2** and their complexes with Na^+, Ag^+, Ca^{2+}, Co^{2+}, Ni^{2+}, Cu^{2+}, Zn^{2+} and Al^{3+} ions were also investigated using DFT calculations at the B3LYP/LanL2DZ theoretical level. The binding strengths of metal ions are, in decreasing order: **L1**/Al^{3+} > > **L1**/Cu^{2+} > **L1**/Ni^{2+} > **L1**/Zn^{2+} > **L1**/Co^{2+} > > **L1**/Ca^{2+} > **L1**/Ag^+ > **L1**/Na^+ for sensor **L1** and **L2**/Al^{3+} > > **L2**/Cu^{2+} > **L2**/Co^{2+} > **L2**/Ni^{2+} > **L2**/Na^+ > **L2**/Zn^{2+} > > **L2**/Ca^{2+} > **L2**/Ag^+ for sensor **L2**. The MLCT data calculated from NBO charge supported the view that Al^{3+} ion has the strongest binding ability with both **L1** and **L2**. The HOMO–LUMO energy level diagrams provided an explanation for the optical properties of complexes from the PET process point of view.

Acknowledgments The authors gratefully acknowledge the faculty of science, Mahasarakham University and the Center of Excellence for Innovation in Chemistry (PERCH-CIC), Thailand for financial support of this research. Profound gratitude is also extended to the facility provided by Supramolecular Chemistry Research Unit and Department of Chemistry, Faculty of Science, Mahasarakham University, Maha Sarakham, Thailand.

References

1. Demchenko AP (2009) Introduction to fluorescence sensing. Springer, Netherlands
2. Jeong Y, Yoon J (2012) Inorg Chim Acta 381:2–14
3. Kaur N, Kumar S (2011) Tetrahedron 67:9233–9264
4. Zhang JF, Zhou Y, Yoon J, Kim JS (2011) Chem Soc Rev 40:3416–3429
5. Zhang X, Shiraishi Y, Hirai T (2007) Tetrahedron Lett 48 (31):5455–5459
6. Huo FJ, Zhang JJ, Yang YT, Chao JB, Yin CX, Zhang YB, Chen TG (2012) Sensors Actuators B Chem 166–167:44–49
7. Li CYL, Xu F, Li YF, Zhou K, Zhou Y (2012) Anal Chim Acta 717:122–126
8. Loudet A, Burgess K (2007) Chem Rev 107(11):4891–4932
9. Benstead M, Mehl GH, Boyle RW (2011) Tetrahedron 67 (20):3573–3601
10. Suzuki S, Kozaki M, Nozaki K, Okada K (2011) J Photochem Photobiol C Photochem Rev 12(4):269–292
11. Boens N, Leen V, Dehaen W (2012) Chem Soc Rev 41:1130–1172
12. Ulrich G, Ziessel R, Harriman A (2008) Angew Chem Int Ed 47:1184–1201
13. Gimpl G, Gehrig-Burger K (2011) Steroids 76(3):216–231
14. Guzow K, Kornowska K, Wiczk W (2009) Tetrahedron Lett 50 (24):2908–2910
15. Mankouri J, Tedbury PR, Gretton S, Hughes ME, Griffin SD, Dallas ML, Green KA, Hardie DG, Peers C, Harris M (2010) Proc Natl Acad Sci USA 107(25):11549–11554
16. Montejano HA, Amat-Guerri F, Costela A, García-Moreno I, Liras M, Sastre R (2006) J Photochem Photobiol A Chem 181(2–3):142–146
17. Badré S, Monnier V, Méallet-Renault R, Dumas-Verdes C, Schmidt EY, Mikhaleva AI, Laurent G, Levi G, Ibanez A, Trofimov BA, Pansu RB (2006) J Photochem Photobiol A Chem 183(3):238–246
18. Yin S, Yuan W, Huang J, Xie D, Liu B, Jiang K, Qiu H (2012) Spectrochim Acta A 96:82–88
19. Kubota Y, Uehara J, Funabiki K, Ebihara M, Matsui M (2010) Tetrahedron Lett 51:6195–6198
20. Lu H, Zhang SS, Liu HZ, Wang YW, Shen Z, Liu CG, You XZ (2009) J Phys Chem A 113(51):14081–14086
21. Valeura B, Leraya I (2000) Coord Chem Rev 205(1):3–40
22. Becke AD (1993) J Chem Phys 98:5648–5652
23. Lee C, Yang W, Parr RG (1988) Phys Rev B 37:785–789
24. Hay PJ, Wadt WR (1985) J Chem Phys 82:270–283
25. Wadt WR, Hay PJ (1985) J Chem Phys 82:284–298
26. Hay PJ, Wadt WR (1985) J Chem Phys 82:299–310
27. Frisch MJ, Trucks GW, Schlegel HB, Scuseria GE, Robb MA, Cheeseman JR, Montgomery JA, Vreven T, Kudin KN, Burant JC, Millam JM, Iyengar SS, Tomasi J, Barone V, Mennucci B, Cossi M, Scalmani G, Rega N, Petersson GA, Nakatsuji H, Hada M, Ehara M, Toyota K, Fukuda R, Hasegawa J, Ishida M, Nakajima T, Honda Y, Kitao O, Nakai H, Klene M, Knox JE, Hratchian HP, Cross JB, Adamo C, Jaramillo J, Gomperts R, Stratmann RE, Yazyev O, Austin AJ, Cammi R, Pomelli C, Ochterski JW, Ayala PY, Morokuma K, Voth GA, Salvador P, Dannenberg JJ, Zakrzewski VG, Dapprich S, Daniels AD, Strain MC, Farkas O, Malick DK, Rabuck AD, Raghavachari K, Foresman JB, Ortiz JV, Cui Q, Baboul AG, Clifford S, Cioslowski J, Stefanov BB, Liu G, Liashenko A, Piskorz P, Komaromi I, Martin RL, Fox DJ, Keith T, Al-Laham MA, Peng CY, Nanayakkara A, Challacombe M, Gill PMW, Johnson B, Chen W, Wong MW, Gonzalez C, Pople JA (2008) Gaussian 03, Revision E01. Gaussian Inc, Wallingford, CT
28. Baruah M, Qin W, Basarić N, De Borggraeve WM, Boens N (2005) J Org Chem 70(10):4152–4157
29. Kennedy DP, Kormos CM, Burdette SC (2009) J Am Chem Soc 131:8578–8586
30. Gabe Y, Urano Y, Kikuchi K, Kojima H, Nagano T (2004) J Am Chem Soc 126:3357–3367
31. Qin W, Baruah M, Van der Auweraer M, Frans C, De Schryver FC, Boens N (2005) J Phys Chem A 109:7371–7384
32. Kollmannsberger M, Rurack K, Resch-Genger U, Daub JJ (1998) Phys Chem A 102:10211–10220
33. Ho T-L (1975) Chem Rev 75:1–20
34. Miessler GL, Tarr DA (2004) Inorganic Chemistry, 3rd edn. Pearson Prentice Hall, New Jersey
35. Chiodo S, Russo N, Sicilia E (2006) J Chem Phys 125:104107–1–104107–8
36. Strassner T, Taige MA (2005) J Chem Theory Comput 1:848–855
37. Ruangpornvisuti V (2007) Struct Chem 18:977–984
38. Remacle F, Grandjean F, Long GJ (2008) Inorg Chem 47:4005–4014
39. Weller A (1968) Pure Appl Chem 16:115–124